ACS APPLIED MATERIALS & INTERFACES

www.acsami.org

Research Article

Microporous Elastomer Filter Coated with Metal Organic Frameworks for Improved Selectivity and Stability of Metal Oxide Gas Sensors

Kyoungjin Hwang,△ Junseong Ahn,△ Incheol Cho, Kyungnam Kang, Kyuyoung Kim, Jungrak Choi, Kyriaki Polychronopoulou, and Inkyu Park*

Cite This: *ACS Appl. Mater. Interfaces* 2020, 12, 13338−13347

Read Online

ACCESS | Metrics & More | Article Recommendations | Supporting Information

ABSTRACT: Despite various advantages and usefulness of semiconductor metal oxide gas sensors, low selectivity and humidity interference have limited their practical applications. In order to resolve these issues, we propose a new concept of a selective gas filtering structure that increases the gas selectivity and decreases the moisture interference of metal oxide gas sensors by coating metal organic frameworks (MOFs) on a microporous elastomer scaffold. Cu(BTC) with an excellent selective adsorption capacity for carbon monoxide (CO) compared to hydrogen (H_2) and MIL-160 with an excellent moisture adsorption capacity were uniformly coated on the microporous polydimethylsiloxane (PDMS) structure through a squeeze coating method, resulting in a high content of MOFs with a large effective surface area. A Cu(BTC)-coated microporous PDMS filter showed an excellent adsorption efficiency (62.4%) for CO, thereby dramatically improving the selectivity of H_2/CO by up to 2.6 times. In addition, an MIL-160 coated microporous PDMS filter showed a high moisture adsorption efficiency (76.2%).

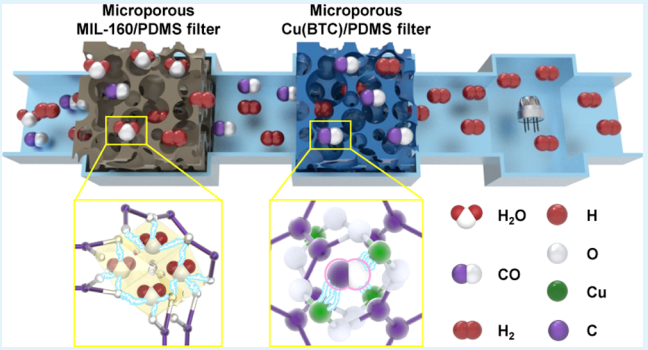

KEYWORDS: *metal oxide gas sensor, gas filter, microporous elastomer, metal organic frameworks, moisture interference*

INTRODUCTION

Semiconductor metal oxide (SMO) gas sensors are being actively applied in various mobile equipment and remote monitoring systems because of many advantages such as high sensitivity, low cost, and compact size.[1−11] Despite these advantages, however, they possess a critical disadvantage of low selectivity because of their sensing principle based on the adsorption and desorption of oxygen gas depending on the environment.[12,13] Because the SMO gas sensors show similar responses between different oxidizing gases or reducing gases, the selectivity between nonidentical gases can be low. Furthermore, because they are sensitive to moisture, the sensing response is highly affected by humidity and the gas selectivity worsens under high humidity conditions.[14] To overcome these drawbacks, various sensing materials such as core−shell nanostructures and multimetallic oxide compounds, functionalization with catalytic nanoparticles, array of multiplexed sensors,[5,15] and gas filtering or separation systems for selective filtration of specific gas molecules have been developed.

In the past, gas filtering or separation techniques have been focused on the development of porous polymer membranes.[16−18] Afterward, selective gas filtering technologies using mixed matrix membranes (MMMs) combined with polymer membranes and metal organic frameworks (MOFs) have been developed for higher gas selectivity.[19−24] In recent years, in situ growth of MOFs onto nanowires[25] and commercial polyurethane (PU) sponges[26] has been developed. However, polymer membranes and MMM require various equipment such as pumps and cylinders to provide high pressure and thus have limitations such as large power consumption and difficulty in miniaturization, making them unsuitable for mobile equipment. On the other hand, in situ growth of MOFs onto nanowires and commercial PU sponges has another limitation: complex and difficult MOF synthesis conditions (temperature, quality, quantity, etc.) on the frame (nanowire, PU sponge, etc.) and low filtering efficiency due to small coating amount of the MOFs.

In this study, we propose a new type of a microporous gas filter by coating the MOFs such as Cu(BTC) and MIL-160 that

Received: January 7, 2020
Accepted: February 19, 2020
Published: February 19, 2020

https://dx.doi.org/10.1021/acsami.0c00143
ACS Appl. Mater. Interfaces 2020, 12, 13338−13347

can selectively absorb gas or moisture onto a microporous polydimethylsiloxane (PDMS) structure that can provide a large surface area and all connected three dimensional multi-microchannels. To implement the microporous gas filter, we used a coating process of presynthesized MOFs (i.e., Cu(BTC) and MIL-160) with high crystallinity on a microporous PDMS structure by the squeeze coating method. This fabrication approach of the microporous gas filter has many advantages. First of all, it is very simple and rapid to fabricate the microporous gas filter, and a large amount of MOFs can be loaded on the filter, so that a high filtering efficiency can be achieved. In addition, the multichannel of the microporous PDMS structure eliminates the need for high pressure to operate the filter, which simplifies the installation and enables low power and miniaturization of the filtering system. By using these structures, we have designed a gas filtering system, as shown in Figure 1. The microporous PDMS filter coated with Cu(BTC)

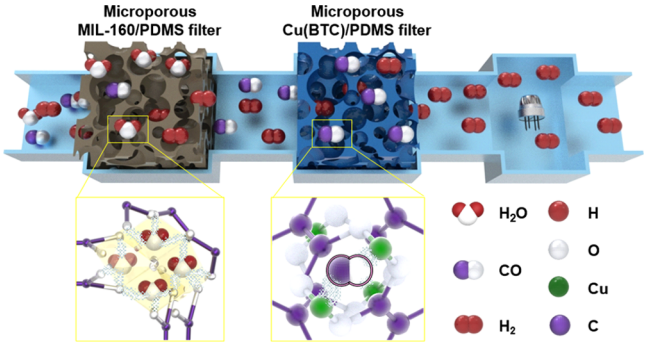

Figure 1. Schematic image of a filtering system based on a microporous elastomer filter coated with MOFs for improving the selectivity for hydrogen (H_2) against carbon monoxide (CO) and minimizing the moisture interference of metal oxide gas sensor. If CO and H_2 are mixed in a humid environment, water (H_2O) molecules are filtered by the microporous MIL-160/PDMS filter, and CO molecules are adsorbed by the microporous Cu(BTC)/PDMS filter, resulting in more selective and stable detection of H_2 in air.

can be used as a gas filter for the selective adsorption of carbon monoxide (CO) in a mixture of CO and H_2, thereby improving the selectivity of the SMO gas sensor for H_2 against CO gas. Meanwhile, the microporous PDMS filter coated with MIL-160 can function as a moisture filter to minimize the interference from humidity by absorbing water (H_2O) molecules.

MOFs are three-dimensional structures in which metal atoms and organic ligands are bonded in a certain pattern. They have been actively studied as next-generation adsorbents and catalysts because of their well-organized and stable crystallinity, high porosity, large surface area, and excellent selective adsorption capacity of gas molecules.[27−31] Among them, Cu(BTC), which is one of the most well-known MOFs, is a structure in which copper (Cu) atoms are connected in a certain pattern by organic ligands, BTC (1,3,5-benzenetricarboxylic acid).[32] These Cu atoms in Cu(BTC) have open metal sites, which provide the catalyzation or adsorption of gas molecules. The adsorption capacities of the Cu(BTC) for various gases have been extensively studied.[33−40] Especially, it has been found that the Cu(BTC) has an excellent adsorption capacity for methane (CH_4), carbon monoxide (CO), carbon dioxide (CO_2),[37] volatile organic compounds (VOCs),[41] and so forth. In addition, utilization of the Cu(BTC) in gas separation, adsorption, and toxic gas removal is being actively studied.[42,43] MIL-160 is a recently developed MOFs formed by combining aluminum (Al) atoms with an organic ligand, FDCA (2,5-furandicarboxylic). The aluminum carboxylate structure of MIL-160 contains a number of oxygen atoms, which not only strengthens hydrophilicity but also maintains the pore volume allowing the H_2O molecules to approach well. Because of this strong hydrophilicity, MIL-160 has been actively studied in applications such as H_2O adsorption/desorption devices for heat pumps and chillers,[44−47] seasonal heat storage systems,[48] and adsorption-driven thermal batteries.[49]

Microporous PDMS structures have been recently studied in energy, sensor, and various other fields, such as water/oil separation,[50,51] micro pumps,[52] flexible pressure sensors,[53] and stretchable ion batteries[54] because of their unique thermal, chemical, mechanical, and structural properties. Especially, microporous PDMS structures fabricated using sugar templates[53,55] have an intermediate structure with the advantages of both open and closed cells, which means that small holes are formed between closed cells so that the they form a multichannel for air to pass easily. Therefore, these microporous PDMS structures offer excellent features as a filter frame, with the advantages of both the large surface area of the closed cell and the multichannel of the open cell.

RESULTS AND DISCUSSION

Fabrication and Characterization of the Microporous Cu(BTC)/PDMS and MIL-160/PDMS Structures. Figure 2 shows the results of the fabricated microporous PDMS structure, microporous Cu(BTC)/PDMS filter, and microporous MIL-160/PDMS filter. The microporous structure of the PDMS (Figure 2a) was well maintained with a porosity of 70.8 ± 2.0% and a pore size of 291 ± 36 μm. As shown in Figure 2b,c, Cu(BTC) and MIL-160 were uniformly coated both inside and outside of the microporous PDMS structure. As shown in Figure 2d−f and Figure S1, MOFs were firmly attached to the porous PDMS surface and the coating materials penetrated well into the inside of microporous PDMS by the squeeze coating process. The crystallinities of each MOFs were well maintained without degradation during the coating process, as shown in the X-ray diffraction (XRD) pattern (Figure 2g,h).[45,56] The weight percentage of Cu(BTC) for the two Cu(BTC)/PDMS filters and the two MIL-160/PDMS filters were measured using their mass changes. One of the two Cu(BTC)/PDMS filters contained 9.82 wt %, while the other sample contained 19.82 wt % of Cu(BTC); on the other hand, one of the microporous MIL-160/PDMS filters contained 18.36 wt %, while the other contained 38.98 wt % MIL-160. In the case of the microporous Cu(BTC)/PDMS filter, the content of Cu(BTC) was 2.75 times higher than that of the previous study in which Cu(BTC) was directly synthesized on a commercial PU sponge.[57]

Characterization of the Microporous Cu(BTC)/PDMS Filters with a Metal Oxide Gas Sensor. Figure 3 shows the results of a gas selectivity test of the microporous Cu(BTC)/PDMS filter. The response of the sensor is defined as $(R_0 - R_g)/R_0$, where R_0 is the resistance of the sensor in the air and R_g is the resistance of the sensor when exposed to the target gas. The adsorption efficiency of the filter is defined as the change in the response of the sensor, which is expressed as follows

$$\text{Adsorption efficiency (\%)} = \left(1 - \frac{S_s}{S_b}\right) \times 100\% \quad (1)$$

https://dx.doi.org/10.1021/acsami.0c00143
ACS Appl. Mater. Interfaces 2020, 12, 13338−13347

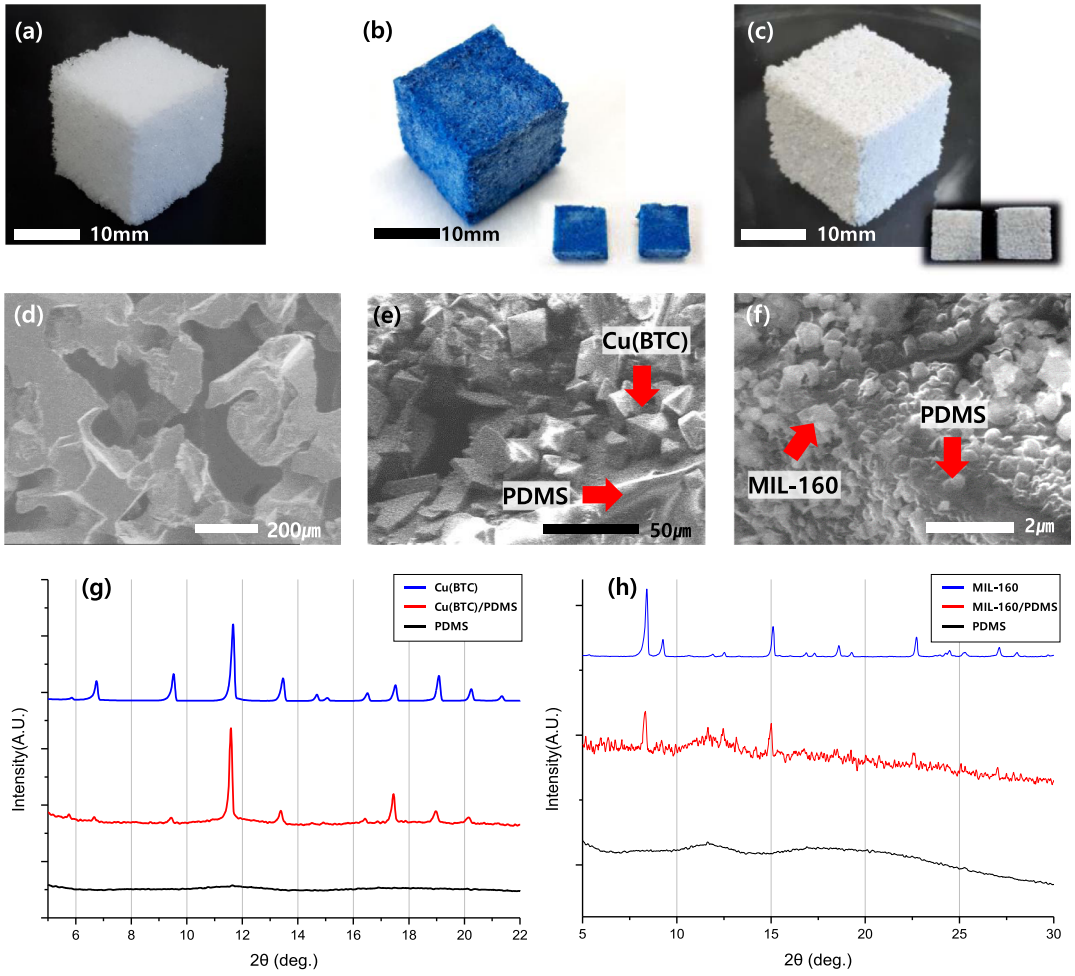

Figure 2. Photographic images of (a) microporous PDMS structure, (b) microporous Cu(BTC)/PDMS filter, (c) microporous MIL-160/PDMS filter, and (d–f) their scanning electron microscopy images (inset images of (b,c) are the cross sections of each filter). XRD patterns of (g) microporous Cu(BTC)/PDMS filter and (h) microporous MIL-160/PDMS filter.

where S_s and S_b are the responses of the sensor with and without a filter mounted in front of the inlet to the sensor. Figure 3a shows the responses of the sensor to the changes in H_2 concentration with various filters, and Figure 3b summarizes the H_2 adsorption capacity of each filter. As shown in these two graphs, there was almost no difference in the sensor response between various filtration conditions. Also, the adsorption efficiencies of each filter were close to zero. From these results, it can be concluded that the microporous Cu(BTC)/PDMS filter has no adsorption capacity for the H_2.

Figure 3c shows the test results of the CO adsorption capacity of the filter. Compared to the response with no filter, the sensor responses to CO gas with 10 wt % and 20 wt % microporous Cu(BTC)/PDMS filters decreased in proportion to the amount of Cu(BTC) within the microporous PDMS matrix. On the other hand, the sensor response did not decrease with the bare microporous PDMS structure (i.e., without Cu(BTC) coating). Figure 3d shows the adsorption efficiency of each filter for CO gas. The adsorption efficiencies of the 10 wt % and 20 wt % microporous Cu(BTC)/PDMS filters were as high as 36.69 and 62.38%, respectively, whereas that of the bare microporous PDMS structure was only 3.68%. Additionally, there was no difference in the sensor response when different sizes of the microporous Cu(BTC)/PDMS filters with the same amount of coated material were used, as shown in Figure S2. These results demonstrate that the microporous PDMS structure itself has a negligible effect on the CO adsorption, while Cu(BTC) coated on the microporous PDMS scaffold has a strong adsorption capability to CO gas, in agreement with the strong affinity of Cu sites for the CO molecule adsorption.

The adsorption capacity of Cu(BTC) for H_2 and CO molecules can be explained by Henry's law. According to Henry's law, the amount of a given gas dissolved in a given type and the volume of solvent is directly proportional to the partial pressure of the gas in equilibrium with the solvent. Here, Henry's constant shows the adsorption capacity of the solvent for the gas molecules. According to Karra and Walton, Henry's constants of Cu(BTC) for H_2 and CO are 0.4×10^{-3} mol/kg·kPa and 9.5×10^{-3} mol/kg·kPa, respectively,[58] resulting in the adsorption capacity of Cu(BTC) for CO much higher than that for H_2 by 24 times. This selective gas adsorption capacity of Cu(BTC) allows the gas sensor to selectively detect H_2 better than CO after gas filtration.

Figure 3e,f presents the improvement of H_2/CO selectivity of the gas sensor due to the selective gas adsorption capacity of the microporous Cu(BTC)/PDMS filter based on the adsorption tests explained above. The selectivity is the ability of a sensor to distinguish target gas against other interfering gases. Thus, the selectivity (K) of H_2 to CO is expressed as S_{H_2}/S_{CO}, where S_{H_2} and S_{CO} are the sensor responses to the H_2 and CO gases,

https://dx.doi.org/10.1021/acsami.0c00143
ACS Appl. Mater. Interfaces 2020, 12, 13338−13347

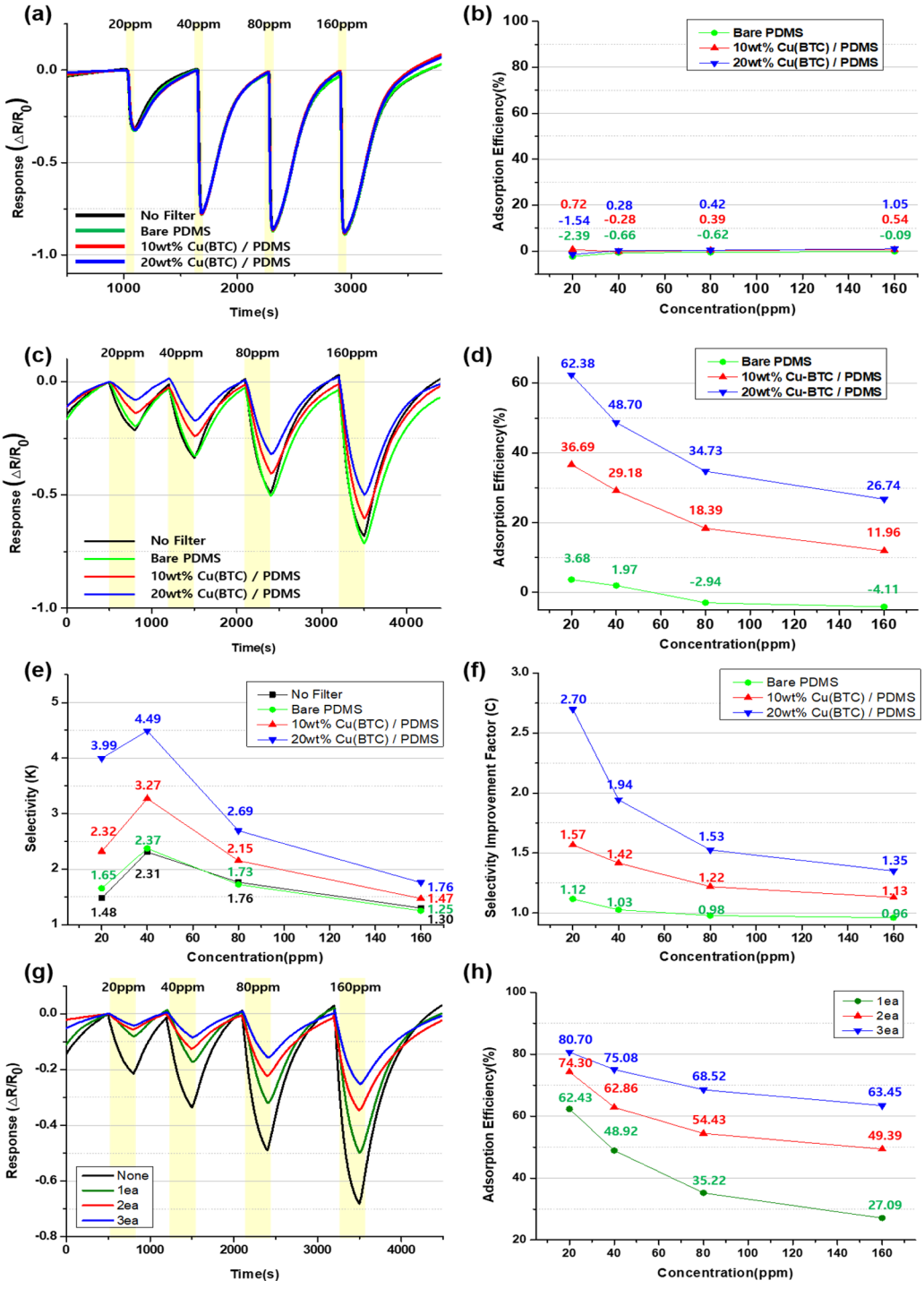

Figure 3. Gas test results of a metal oxide gas sensor with microporous Cu(BTC)/PDMS filters. (a) Sensor response to H_2 gas, (b) adsorption efficiency for H_2 gas, (c) sensor response to CO gas, (d) adsorption efficiency for CO gas, (e) selectivity for H_2/CO gases, (f) selectivity improvement factor, (g) sensor response to CO gas, and (h) adsorption efficiency for CO with insertions of one, two, and three filters in series.

respectively. In order to evaluate how much the selectivity increases by introducing the microporous Cu(BTC)/PDMS filter, the selectivity improvement factor is defined as follows.

$$\text{Selectivity improvement factor } (C) = \frac{K_s}{K_n} \quad (2)$$

where K_s is the selectivity of H_2 to CO when 0, 10, and 20 wt % microporous Cu(BTC)/PDMS filters are utilized and K_n is the selectivity of the gas sensor without using any filter. When the microporous Cu(BTC)/PDMS filters were utilized, the selectivity increased by 1.57 times and 2.70 times with 10 wt % and 20 wt % of Cu(BTC) contents, respectively. These results show that the microporous Cu(BTC)/PDMS filter can improve the selectivity of H_2 to CO.

Furthermore, the developed filter shows excellent reliability in the tests for reproducibility and long-term stability. The standard deviation of CO adsorption efficiency between five different filters at each concentration is lower than 5% (maximum deviation = 4.65% under 20 ppm CO gas), as

https://dx.doi.org/10.1021/acsami.0c00143
ACS Appl. Mater. Interfaces 2020, 12, 13338−13347

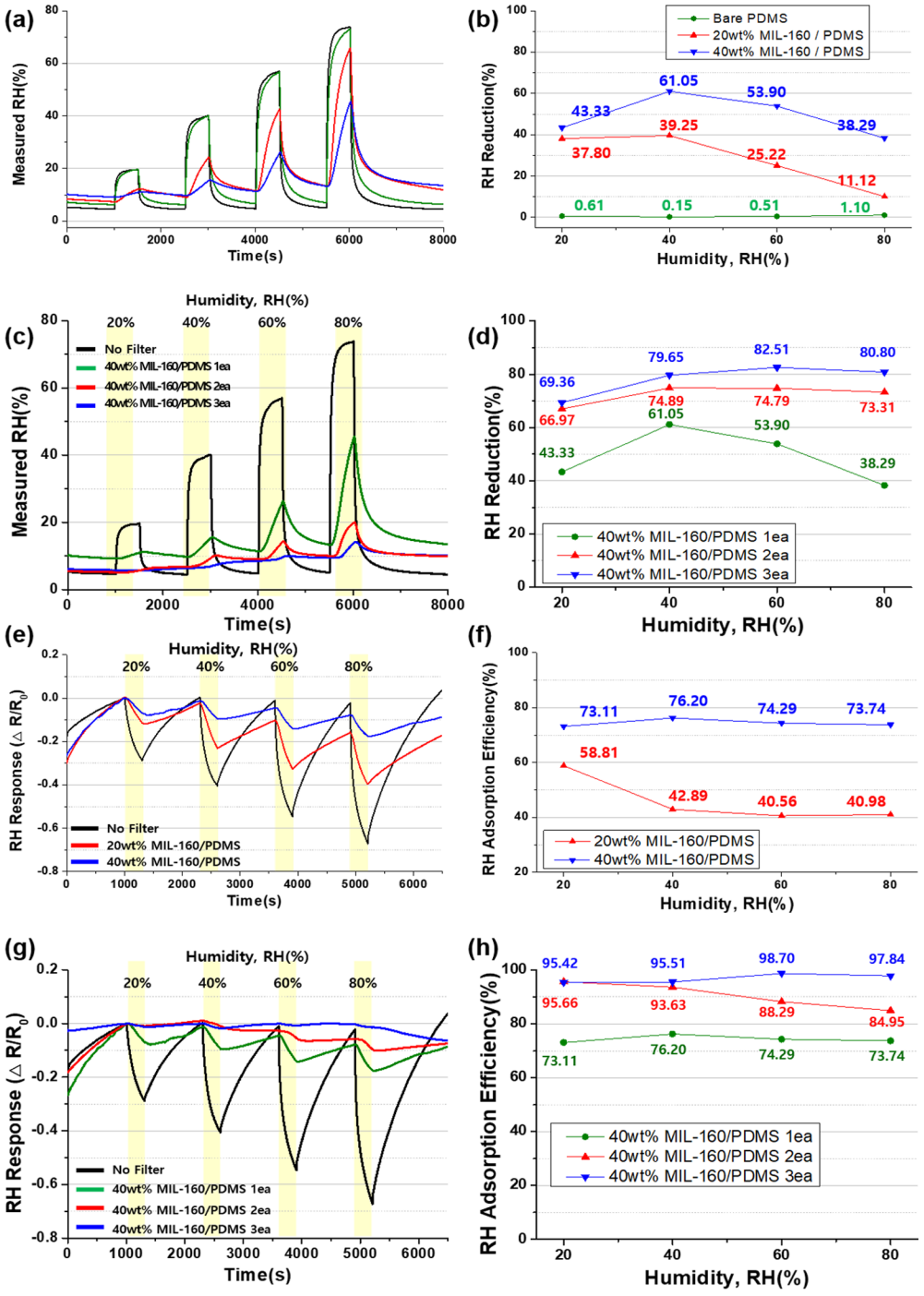

Figure 4. Reduction of the RH effect by the microporous MIL-160/PDMS filters with an RH sensor (a–d) and a metal oxide gas sensor (e–h): (a,b) response of a RH sensor (a) and RH reduction (b) by bare microporous PDMS filter, 20 wt % microporous MIL-160/PDMS filter, and 40 wt % microporous MIL-160/PDMS filter; (c,d) response of a RH sensor (c) and RH reduction (d) by the insertions of one, two, and three 40 wt % microporous MIL-160/PDMS filters in series; (e,f) response of a metal oxide gas sensor (e) and adsorption efficiency (f) of bare microporous PDMS filter, 20 wt % microporous MIL-160/PDMS filter, and 40 wt % microporous MIL-160/PDMS filter; (g,h) response of a metal oxide gas sensor (g) and adsorption efficiency (h) by insertions of one, two, and three 40 wt % microporous MIL-160/PDMS filters in series.

shown in Figure S3. The sensor response also did not change over time, which means there is no degradation of the adsorption efficiency of the filters, as shown in Figure S4. These results show that the developed filter can improve the selectivity of a metal oxide gas sensor without a trade-off in reproducibility and long-term stability.

Figure 3g,h present the change of the response and the adsorption efficiency for CO gas of the sensor when two or three microporous filters are connected in series. As shown in these two figures, when the number of mounted filters increases, the response of the sensor to CO gas decreases and the adsorption efficiency increases accordingly. Here, lower adsorption efficiency for higher CO concentration is partially resolved using a series of several filters. After the insertion of three filters, the adsorption efficiency did not decrease rapidly even at a high

https://dx.doi.org/10.1021/acsami.0c00143
ACS Appl. Mater. Interfaces 2020, 12, 13338–13347

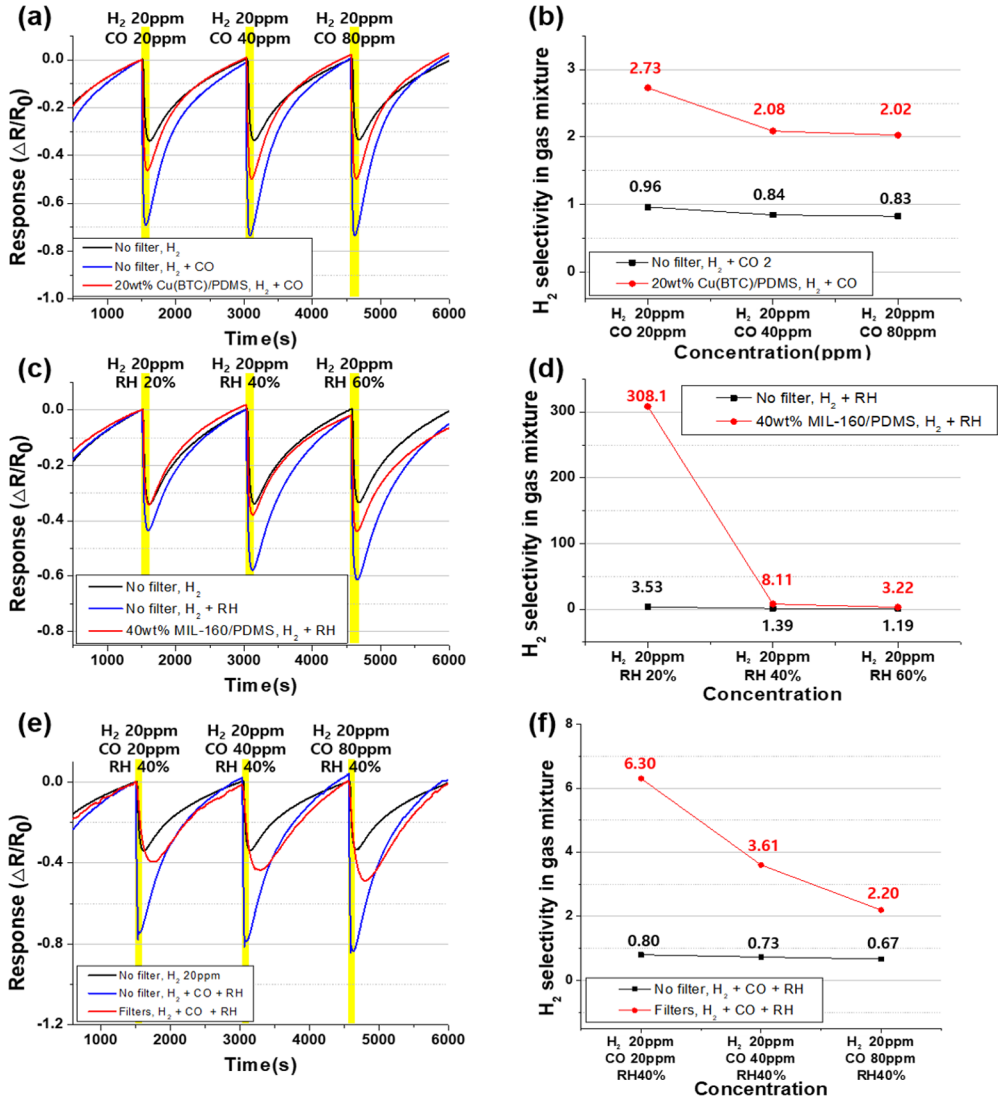

Figure 5. Gas test results of the mixture of (a,b) H_2 and CO gas with Cu(BTC)/PDMS filter, (c,d) H_2 and humid air with MIL-160/PDMS filter, and (e,f) H_2, CO, and humid air with both filters: (a) H_2 sensor response and (b) selectivity to the mixture of 20 ppm H_2 and 20/40/80 ppm CO gas with/without microporous Cu(BTC)/PDMS filter. (c) H_2 sensor response and (d) selectivity to the mixture of 20 ppm H_2 gas and RH 20/40/60% air with/without microporous MIL-160/PDMS filter. (e) H_2 sensor response and (f) selectivity to the mixture of 20 ppm H_2 gas, RH 40% air, and 20/40/60 ppm CO gas with/without microporous Cu(BTC)/PDMS and MIL-160/PDMS filters.

concentration of 160 ppm CO gas and remained high at more than 63%.

Characterization of the Microporous MIL-160/PDMS Filters with a Metal Oxide Gas Sensor. Figure 4 shows the humidity adsorption test results for the microporous MIL-160/PDMS filter. In Figure 4a, relative humidity (RH) is measured by the humidity sensor for input RHs of 20, 40, 60, and 80%. Here, "input RH (%)" is the set RH controlled by the experimental setup, and "measured RH (%)" is the RH after filtration measured by the humidity sensor. Figure 4b is a graph summarizing the effect of the RH reduction by the microporous MIL-160/PDMS filter, and the degree of the RH reduction (RH reduction) is defined as follows.

$$\text{RH reduction (\%)} = \left(1 - \frac{\text{measured RH (\%)}_s}{\text{measured RH (\%)}_n}\right) \times 100\% \quad (3)$$

where "measured RH $(\%)_n$" is measured RH when the filter is not inserted and "measured RH $(\%)_s$" is measured RH when the filter is inserted. In addition, "RH reduction (%)" refers to the degree of RH reduction when the filter is inserted as compared to when the filter is not inserted.

These two graphs show that when 20 and 40 wt % microporous MIL-160/PDMS filters were inserted, the RH was significantly reduced as compared to the value measured without filter. The RH reduction by each filter increased more as the amount of coated MIL-160 increased. RH reduction by 20 wt % and 40 wt % microporous MIL-160/PDMS filters was 39.3 and 61.1%, respectively. However, with microporous MIL-160/PDMS filter, the sensor response was not recovered quickly when dry air was injected. This is because the moisture adsorbed by the microporous MIL-160/PDMS filter did not quickly escape from the filter. The more the amount of coated MIL-160, the longer the injection time of the humid air, and the more the number of mounted filters, the longer the recovery time became. The problem with this long recovery time can be solved by heating and drying the filter; details of the design and demonstration are provided in Figure S5. Figure 4c,d shows

https://dx.doi.org/10.1021/acsami.0c00143
ACS Appl. Mater. Interfaces 2020, 12, 13338−13347

the changes of the RH and RH reduction when 1, 2, and 3 microporous MIL-160/PDMS filters were mounted. As the number of filters increased, the RH reduction also increased. When three filters were mounted in series, the maximum RH reduction rate was 82%.

Figure 4e,f presents the change of baseline resistance of the metal oxide gas sensor under various RHs to confirm the moisture removal effect of the microporous MIL-160/PDMS filter for the gas sensor. As shown in these figures, the response of the metal oxide gas sensor to RH was significantly reduced when the microporous MIL-160/PDMS filter was mounted (Figure 4e). The adsorption efficiency of the 20 wt % microporous MIL-160/PDMS filter was up to 40% and that of the 40 wt % microporous MIL-160/PDMS filter was up to 68% (Figure 4f). Similar to the Cu(BTC) filters, the adsorption efficiency was only affected by the total amount of the coating material (i.e., MIL-160) not the filter size, as shown in Figure S6. Furthermore, the adsorption efficiency dramatically increased as the number of filters increased, and the adsorption efficiency increased up to 98.7% when three filters were mounted in series (see Figure 4g,h). On the other hand, as in the previous humidity sensor test, the sensing delay of the gas sensor occurred by the insertion of the filter. Detection delay time of about 30 s occurred when one filter was mounted. As the number of filters increased, the detection delay time became longer. When three filters were mounted, the detection time was delayed by about 100 s.

Finally, the reproducibility of the MIL-160/PDMS filter was investigated. The standard deviation of RH adsorption efficiency between five different filters at each concentration was lower than 6% (maximum deviation = 5.53% under RH 20%), and the change of the adsorption efficiency after 3 months was negligible (deviation <3%), as shown in Figures S7 and S8, respectively. This excellent reproducibility can be attributed to the repeatable coating process of MOFs and good adhesion between microporous PDMS and MIL-160.

Performance of the Microporous Cu(BTC)/PDMS and MIL-160/PDMS Filters with a Metal Oxide Gas Sensor. Figure 5 shows the results of the gas selectivity test with the microporous Cu(BTC)/PDMS and MIL-160/PDMS filters to the mixtures of H_2, CO, and humid air. In order to evaluate the filtering performance, the H_2 selectivity was defined as the change in the sensor response to the pure H_2 and gas mixture, which is expressed as follows

$$H_2 \text{ selectivity in gas mixture} = \left(\frac{S_{H_2}}{S_{\text{mixture}} - S_{H_2}} \right) \quad (4)$$

where S_{H_2} and S_{mixture} are the responses ($\Delta R/R_0$) of the sensor to pure H_2 gas and the gas mixture, respectively. Figure 5a shows the response of the metal oxide gas sensor to the mixture of 20 ppm H_2 and 20/40/80 ppm CO gas. The sensor responses to the mixture of 20 ppm H_2 and 20/40/80 ppm CO gas (S_{mixture} = −0.69, −0.74, and −0.74 to 20, 40, and 80 ppm CO, respectively) was higher than that to the pure 20 ppm H_2 gas (S_{H_2} = −0.34) because the metal oxides react with both H_2 and CO gas and both have reducing nature. On the other hand, the sensor response with the microporous Cu(BTC)/PDMS filter (S_{mixture} = −0.46, −0.50, and −0.50 to 20, 40, and 80 ppm CO, respectively) showed relatively a small difference with the response to pure H_2 gas (S_{H_2} = −0.34) because the filter effectively captured the interfering CO molecules in the mixture gas. In summary, the H_2 selectivity was improved by 2.44−2.84 times with the Cu(BTC)/PDMS filter, as shown in Figure 5b.

Figure 5c shows the response of the metal oxide gas sensor to the mixture of 20 ppm H_2 gas and RH 20/40/60% air. The sensor responses to the mixture gas (S_{mixture} = −0.43, −0.58, and −0.61 to RH 20, 40, and 60% air, respectively) was also higher than that to the pure 20 ppm H_2 gas (S_{H_2} = −0.34) because of the interference by humidity, and the interference effect of humid air was reduced by using the microporous MIL-160/PDMS filter (S_{mixture} = −0.34, −0.38, and −0.44 to RH 20, 40, and 60% air, respectively). The H_2 selectivity to RH 20, 40, and 60% air was improved by 87.2, 5.83, and 2.70 times with the MIL-160/PDMS filter, as shown in Figure 5d. Notably, in the low humidity region (i.e., RH 20% air), most of the moisture in the atmosphere was captured by the filter, resulting in a significantly enhanced selectivity. In contrast, the performance of the filtering system was relatively deteriorated in the high humidity region because of the limited adsorption capacity of MOFs. This problem can be resolved by increasing the total amount of MOF materials (e.g., by increasing the size, number, and MOF concentration of the filter), as discussed in the previous section. Furthermore, in case of prolonged exposure to high humidity or CO concentration, replacement with new filters on a regular basis will prevent the problem of filter saturation.

Finally, the sensor response to the mixture of H_2 gas, CO gas, and humid air was investigated to prove the performance of the filtering system in terms of selectivity against CO and stability against the moisture interference. In the filtering system, water molecules are filtered by the microporous MIL-160/PDMS filter first and CO molecules are adsorbed by the microporous Cu(BTC)/PDMS filter. According to previous studies, Cu(BTC) is not stable under certain humid conditions (RH maintained higher than 30% at 25 °C).[36] Therefore, the degradation of Cu(BTC) should be prevented by installing an MIL-160/PDMS filter, which can adsorb water molecules, in front of the Cu(BTC)/PDMS filter, as shown in Figure 1. As shown in Figure 5e, the interfering effects of CO and humid air were clearly reduced by inserting both the Cu(BTC)/PDMS and MIL-160/PDMS filters. The H_2 selectivity to the mixture of 20 ppm H_2 gas, RH 40% air, and 20/40/80 ppm CO gas was improved by 7.87, 4.94, and 3.29 times, respectively, by using both filters, as shown in Figure 5f. Therefore, it can be concluded that our proposed MOF-loaded microporous elastomer filters can be simultaneously integrated into the gas detecting system for reducing the interfering effects of CO and humidity, resulting in a more selective and stable detection of H_2 gas.

CONCLUSIONS

In summary, we have proposed novel microporous gas filters based on the 3D microporous elastomer coated with MOFs to improve the gas selectivity and to minimize the moisture interference of metal oxide gas sensor. The microporous PDMS structure functions as an excellent filter frame because of its easy fabrication and structural advantages such as three-dimensional multimicrochannel, large surface area, and so forth. The MOFs (Cu(BTC) and MIL-160) were coated by a simple and rapid squeeze coating method. In addition to the MOFs mentioned in this study, various other functional materials can be coated and used as a multipurpose filter. This filter has the advantage that it requires less pressure and equipment than the conventional membrane filter, and the manufacturing process is very simple. In particular, the microporous Cu(BTC)/PDMS filter was able

https://dx.doi.org/10.1021/acsami.0c00143
ACS Appl. Mater. Interfaces 2020, 12, 13338−13347

to exhibit high performance by containing about 2.75 times more contents of Cu(BTC) than the method of in situ growth on the commercial PU sponge.

The gas sensing test with the Cu(BTC)-coated microporous PDMS filter proved that the response of the sensor to H_2 gas did not get affected, while that to CO gas considerably decreased. As a result, the use of the microporous Cu(BTC)/PDMS filter could dramatically improve the selectivity of the metal oxide gas sensor for H_2 gas against CO gas. In the case of MIL-160-coated microporous PDMS filter, which has an excellent adsorption capacity to the moisture, the RH was reduced by up to 61.05%. Also, the metal oxide gas sensor test result showed a high adsorption efficiency of 76.20% for moisture. When three filters were assembled together in series, the filter showed a very high adsorption efficiency of 98% and interference from moisture was negligible. We believe that the proposed microporous PDMS filters coated with MOFs can be utilized in various gas sensing applications such as hydrogen energy systems (e.g., hydrogen fuel cell), medical diagnosis systems (e.g., breath detection-based disease diagnosis), and environmental monitoring systems (e.g., air pollution sensing) that require high selectivity and stability in a humid environment.

METHODS

Preparation of Microporous PDMS Structure. Microporous PDMS structure was fabricated using the process introduced in our previous works.[53,55] As shown in Figure S9, a sugar cube was immersed in the mixture of PDMS pre-polymer and curing agent (weight ratio of 10:1). Then the pre-polymer was completely absorbed in the sugar cube under vacuum for 1 h. After curing in an oven at 70 °C for 3 h, PDMS on the surface of a sugar cube was removed to expose the sugar to outer surface. Then, sugar was dissolved in DI water for 24 h. After additional washing with DI water and drying at 60 °C in a vacuum oven for 24 h, microporous PDMS structure was obtained.

Synthesis of Cu(BTC) and MIL-160. The synthesis method of Cu(BTC) was introduced by Schlichte, et al.[59] Figure S10a is a schematic image of the synthesis process of Cu(BTC). Copper(II) nitrate trihydrate ($Cu(NO_3)_2{\cdot}3H_2O$) (1.53 g) was dissolved in 25 mL of DI water, and 0.89 g of trimecic acid ($C_6H_3(CO_2H)_3$) was dissolved in 25 mL of ethanol. These two solutions were mixed under stirring conditions for 30 min at room temperature. Then, a well-mixed precursor was placed in an autoclave and Cu(BTC) was hydrothermally synthesized at 120 °C for 24 h. After filtration and washing it with ethanol, synthesized blue crystal of Cu(BTC) was dried in a vacuum oven at 100 °C for 24 h.

The synthesis of MIL-160 was conducted using the method proposed by Cadiau, et al.[44] Figure S10b shows the synthesis process of MIL-160. FDCA (2,5-furandicarboxylic acid) (4.69 g), 7.24 g of aluminum chloride hexahydrate ($AlCl_3{\cdot}6H_2O$), and 1.2 g of sodium hydroxide (NaOH) were dissolved in 20 mL of DI water. The solutions were mixed in a round-bottom flask and heated at 100 °C with magnetic stirring for 24 h. After being cooled down to the room temperature, the product was filtered and washed with ethanol. Then, beige-colored MIL-160 was obtained after 24 h of drying at 100 °C in a vacuum oven.

Coating of Cu(BTC) and MIL-160 onto a Microporous PDMS Structure. The synthesized MOFs were coated onto the microporous PDMS structure by squeeze−coating, as shown in Figure S11. First, each MOF was fully dispersed in 5 mL of ethanol by sonication. Then, the microporous PDMS structure was immersed in the solution and squeezed several times until the solution was fully absorbed. The MOF-adsorbed filter was dried at room temperature in air for 1 h and then further dried in a vacuum oven for 24 h to completely remove the residual solvent. As a result, 10 and 20 wt % of Cu(BTC) and 20 and 40 wt % of MIL-160 were coated onto the microporous PDMS structure, considering the pore volume of the microporous PDMS structure and the densities of Cu(BTC) (0.35 g/cm^3) and MIL-160 (1.097 g/cm^3).

Gas Sensing Test Method and Procedure. We conducted gas sensing tests to determine the effect of selective CO adsorption capacity of the microporous Cu(BTC)/PDMS filter and the moisture adsorption capacity of the microporous MIL-160/PDMS filter for the improvement of the selectivity and the removal of moisture interference of the sensor, respectively. A commercial metal oxide gas sensor (MQ-5, Zhengzhou Winsen Electronics Technology Co., China) based on a SnO_2 thin film as the sensing material was commonly used for the gas and humidity test. In addition, by conducting a humidity test using a humidity sensor as well as a gas sensor, the humidity adsorption effect of the microporous MIL-160/PDMS filter was quantitatively confirmed. The microporous PDMS structures with/without Cu(BTC) and MIL-160 were inserted into a filter holder made using a 3D printer. Then, the filter holder was installed in front of the inlet side of the sensor chambers with dimensions of 100 mm × 70 mm × 65 mm for the CO gas test and 112 mm × 47 mm × 20 mm for the humidity test. The ambient temperature was maintained at 23 °C during the entire gas test. The detailed schematic illustration of the experimental setup for the abovementioned gas sensor test is provided in Figure S12. Additionally, a membrane heater for the drying process of the microporous MIL-160/PDMS filter was fabricated following a fabrication process of the previously reported flexible membrane heater.[60,61] Using the test results with gas sensors and humidity sensors, we compared the selective adsorption performances of various microporous filters.

ASSOCIATED CONTENT

Supporting Information

The Supporting Information is available free of charge at https://pubs.acs.org/doi/10.1021/acsami.0c00143.

Reproducibility and uniformity of the developed gas filters, detailed fabrication methods of MOFs materials, and experimental setup for the gas test (PDF)

AUTHOR INFORMATION

Corresponding Author

Inkyu Park − *Department of Mechanical Engineering, Korea Advanced Institute of Science and Technology (KAIST), Daejeon 34141, Republic of Korea*; orcid.org/0000-0001-5761-7739; Phone: +82-42-350-3240; Email: inkyu@kaist.ac.kr; Fax: +82-42-350-3210

Authors

Kyoungjin Hwang − *Department of Mechanical Engineering, Korea Advanced Institute of Science and Technology (KAIST), Daejeon 34141, Republic of Korea*

Junseong Ahn − *Department of Mechanical Engineering, Korea Advanced Institute of Science and Technology (KAIST), Daejeon 34141, Republic of Korea*

Incheol Cho − *Department of Mechanical Engineering, Korea Advanced Institute of Science and Technology (KAIST), Daejeon 34141, Republic of Korea*

Kyungnam Kang − *Department of Mechanical Engineering, Korea Advanced Institute of Science and Technology (KAIST), Daejeon 34141, Republic of Korea*

Kyuyoung Kim − *Department of Mechanical Engineering, Korea Advanced Institute of Science and Technology (KAIST), Daejeon 34141, Republic of Korea*

Jungrak Choi − *Department of Mechanical Engineering, Korea Advanced Institute of Science and Technology (KAIST), Daejeon 34141, Republic of Korea*

Kyriaki Polychronopoulou − *Department of Nano Manufacturing Technology, Khalifa University, Abu Dhabi 127788, United Arab Emirates*

Complete contact information is available at:

https://dx.doi.org/10.1021/acsami.0c00143
ACS Appl. Mater. Interfaces 2020, 12, 13338−13347

https://pubs.acs.org/10.1021/acsami.0c00143

Author Contributions

△K.H. and J.A. contributed equally. The manuscript was written through contributions of all authors. All authors have given approval to the final version of the manuscript.

Notes

The authors declare no competing financial interest.

■ ACKNOWLEDGMENTS

This work was supported by the National Research Foundation of Korea (NRF) grant funded by the Korea government (MSIT) (no. 2018R1A2B2004910) and by KUSTAR-KAIST Institute (KKI).

■ REFERENCES

(1) Sberveglieri, G.; Hellmich, W.; Müller, G. Silicon hotplates for metal oxide gas sensor elements. *Microsyst. Technol.* **1997**, *3*, 183−190.
(2) Simon, I.; Bârsan, N.; Bauer, M.; Weimar, U. Micromachined metal oxide gas sensors: Opportunities to improve sensor performance. *Sens. Actuators, B* **2001**, *73*, 1−26.
(3) Meixner, H.; Lampe, U. Metal oxide sensors. *Sens. Actuators, B* **1996**, *33*, 198−202.
(4) Eranna, G.; Joshi, B. C.; Runthala, D. P.; Gupta, R. P. "Oxide Materials for Development of Integrated Gas Sensors—A Comprehensive Review. *Crit. Rev. Solid State Mater. Sci.* **2004**, *29*, 111−188.
(5) Hierlemann, A. Integrated chemical microsensor systems in CMOS-technology. In *The 13th International Conference on Solid-State Sensors, Actuators and Microsystems, 2005. Digest of Technical Papers. TRANSDUCERS '05*, 2005; Vol. *2*, pp 1134−1137.
(6) Sun, Y.-F.; Liu, S.-B.; Meng, F.-L.; Liu, J.-Y.; Jin, Z.; Kong, L.-T.; Liu, J.-H. Metal Oxide Nanostructures and Their Gas Sensing Properties: A Review. *Sensors* **2012**, *12*, 2610−2631.
(7) Götz, A.; Gràcia, I.; Cané, C.; Lora-Tamayo, E.; Horrillo, M. C.; Getino, J.; García, C.; Gutiérrez, J. A micromachined solid state integrated gas sensor for the detection of aromatic hydrocarbons. *Sens. Actuators, B* **1997**, *44*, 483−487.
(8) Fine, G. F.; Cavanagh, L. M.; Afonja, A.; Binions, R. Metal oxide semi-conductor gas sensors in environmental monitoring. *Sensors* **2010**, *10*, 5469−5502.
(9) Arafat, M. M.; Dinan, B.; Akbar, S. A.; Haseeb, A. S. M. A. Gas sensors based on one dimensional nanostructured metal-oxides: A review. *Sensors* **2012**, *12*, 7207−7258.
(10) Varghese, O. K.; Grimes, C. A. Metal Oxide Nanoarchitectures for Environmental Sensing. *J. Nanosci. Nanotechnol.* **2003**, *3*, 277−293.
(11) Ramgir, N.; Datta, N.; Kaur, M.; Kailasaganapathi, S.; Debnath, A. K.; Aswal, D. K.; Gupta, S. K. Metal oxide nanowires for chemiresistive gas sensors: Issues, challenges and prospects. *Colloids Surf., A* **2013**, *439*, 101−116.
(12) Neri, G. First Fifty Years of Chemoresistive Gas Sensors. *Chemosensors* **2015**, *3*, 1−20.
(13) Shankar, P.; Bosco, J.; Rayappan, B. "Gas sensing mechanism of metal oxides : The role of ambient atmosphere, type of semiconductor and gases - A review. *Sci. Lett.* **2015**, *4*, 126.
(14) Shaik, M.; Rao, V. K.; Gupta, M.; Murthy, K. S. R. C.; Jain, R. Chemiresistive gas sensor for the sensitive detection of nitrogen dioxide based on nitrogen doped graphene nanosheets. *RSC Adv.* **2016**, *6*, 1527−1534.
(15) Suh, J.-H.; Cho, I.; Kang, K.; Kweon, S.-J.; Lee, M.; Yoo, H.-J.; Park, I. Fully integrated and portable semiconductor-type multi-gas sensing module for IoT applications. *Sens. Actuators, B* **2018**, *265*, 660−667.
(16) Baker, R. W. Future directions of membrane gas separation technology. *Ind. Eng. Chem. Res.* **2002**, *41*, 1393−1411.
(17) Sridhar, S.; Bee, S.; Bhargava, S. K. Membrane-based Gas Separation: Principle, Applications and Future Potential. *Chem. Eng. Dig.* **2014**, 1−25.
(18) Scholes, C. A.; Stevens, G. W.; Kentish, S. E. Membrane gas separation applications in natural gas processing. *Fuel* **2012**, *96*, 15−28.
(19) Denny, M. S.; Cohen, S. M. In Situ Modification of Metal-Organic Frameworks in Mixed-Matrix Membranes. *Angew. Chem., Int. Ed.* **2015**, *54*, 9029−9032.
(20) Tanh Jeazet, H. B.; Staudt, C.; Janiak, C. Metal-organic frameworks in mixed-matrix membranes for gas separation. *Dalton Trans.* **2012**, *41*, 14003−14027.
(21) Chung, T.-S.; Jiang, L. Y.; Li, Y.; Kulprathipanja, S. Mixed matrix membranes (MMMs) comprising organic polymers with dispersed inorganic fillers for gas separation. *Prog. Polym. Sci.* **2007**, *32*, 483−507.
(22) Basu, S.; Maes, M.; Cano-Odena, A.; Alaerts, L.; De Vos, D. E.; Vankelecom, I. F. J. Solvent resistant nanofiltration (SRNF) membranes based on metal-organic frameworks. *J. Membr. Sci.* **2009**, *344*, 190−198.
(23) Goh, P. S.; Ismail, A. F.; Sanip, S. M.; Ng, B. C.; Aziz, M. Recent advances of inorganic fillers in mixed matrix membrane for gas separation. *Sep. Purif. Technol.* **2011**, *81*, 243−264.
(24) Aroon, M. A.; Ismail, A. F.; Matsuura, T.; Montazer-Rahmati, M. M. Performance studies of mixed matrix membranes for gas separation: A review. *Sep. Purif. Technol.* **2010**, *75*, 229−242.
(25) Drobek, M.; Kim, J.-H.; Bechelany, M.; Vallicari, C.; Julbe, A.; Kim, S. S. MOF-Based Membrane Encapsulated ZnO Nanowires for Enhanced Gas Sensor Selectivity. *ACS Appl. Mater. Interfaces* **2016**, *8*, 8323−8328.
(26) Li, H.; Li, M.; Li, W.; Yang, Q.; Li, Y.; Gu, Z.; Song, Y. Three dimensional MOF-sponge for fast dynamic adsorption. *Phys. Chem. Chem. Phys.* **2017**, *19*, 5746−5752.
(27) Mueller, U.; Schubert, M.; Teich, F.; Puetter, H.; Schierle-Arndt, K.; Pastré, J. "Metal−organic frameworks—prospective industrial applications. *J. Mater. Chem.* **2006**, *16*, 626−636.
(28) Champness, N. R. The future of metal-organic frameworks. *Dalton Trans.* **2011**, *40*, 10311−10315.
(29) Farrusseng, D.; Aguado, S.; Pinel, C. Metal-organic frameworks: Opportunities for catalysis. *Angew. Chem., Int. Ed.* **2009**, *48*, 7502−7513.
(30) Huxford, R. C.; Della Rocca, J.; Lin, W. Metal-organic frameworks as potential drug carriers. *Curr. Opin. Chem. Biol.* **2010**, *14*, 262−268.
(31) Silva, C. G.; Corma, A.; García, H. Metal-organic frameworks as semiconductors. *J. Mater. Chem.* **2010**, *20*, 3141−3156.
(32) Karra, J. R.; Walton, K. S. Effect of Open Metal Sites on Adsorption of Polar and Nonpolar Molecules in Metal−Organic Framework Cu-BTC. *Langmuir* **2008**, *24*, 8620−8626.
(33) Wang, Q. M.; Shen, D.; Bülow, M.; Lau, M. L.; Deng, S.; Fitch, F. R.; Lemcoff, N. O.; Semanscin, J. Metallo-organic molecular sieve for gas separation and purification. *Microporous Mesoporous Mater.* **2002**, *55*, 217−230.
(34) Vishnyakov, A.; Ravikovitch, P. I.; Neimark, A. V.; Bülow, M.; Wang, Q. M. "Nanopore structure and sorption properties of Cu− BTC metal− organic framework. *Nano Lett.* **2003**, *3*, 713−718.
(35) Panella, B.; Hirscher, M.; Pütter, H.; Müller, U. Hydrogen adsorption in metal-organic frameworks: Cu-MOFs and Zn-MOFs compared. *Adv. Funct. Mater.* **2006**, *16*, 520−524.
(36) Liang, Z.; Marshall, M.; Chaffee, A. L. CO2 adsorption-based separation by metal organic framework (Cu-BTC) versus zeolite (13X). *Energy Fuels* **2009**, *23*, 2785−2789.
(37) Chowdhury, P.; Mekala, S.; Dreisbach, F.; Gumma, S. Adsorption of CO, CO2and CH4on Cu-BTC and MIL-101 metal organic frameworks: Effect of open metal sites and adsorbate polarity. *Microporous Mesoporous Mater.* **2012**, *152*, 246−252.
(38) Achmann, S.; Hagen, G.; Kita, J.; Malkowsky, I.; Kiener, C.; Moos, R. Metal-Organic frameworks for sensing applications in the gas phase. *Sensors* **2009**, *9*, 1574−1589.
(39) Gutiérrez-Sevillano, J. J.; Vicent-Luna, J. M.; Dubbeldam, D.; Calero, S. Molecular mechanisms for adsorption in Cu-BTC metal organic framework. *J. Phys. Chem. C* **2013**, *117*, 11357−11366.
(40) Liu, J.; Culp, J. T.; Natesakhawat, S.; Bockrath, B. C.; Zande, B.; Sankar, S. G.; Garberoglio, G.; Johnson, J. K. Experimental and

theoretical studies of gas adsorption in Cu 3(BTC) 2: An effective activation procedure. *J. Phys. Chem. C* **2007**, *111*, 9305−9313.
(41) Homayoonnia, S.; Zeinali, S. Design and fabrication of capacitive nanosensor based on MOF nanoparticles as sensing layer for VOCs detection. *Sens. Actuators, B* **2016**, *237*, 776−786.
(42) Barea, E.; Montoro, C.; Navarro, J. A. R. Toxic gas removal-metal-organic frameworks for the capture and degradation of toxic gases and vapours. *Chem. Soc. Rev.* **2014**, *43*, 5419−5430.
(43) Ebrahim, A. M.; Jagiello, J.; Bandosz, T. J. Enhanced reactive adsorption of H2S on Cu-BTC/ S- and N-doped GO composites. *J. Mater. Chem. A* **2015**, *3*, 8194−8204.
(44) Cadiau, A.; Lee, J. S.; Damasceno Borges, D.; Fabry, P.; Devic, T.; Wharmby, M. T.; Martineau, C.; Foucher, D.; Taulelle, F.; Jun, C.-H.; Hwang, Y. K.; Stock, N.; De Lange, M. F.; Kapteijn, F.; Gascon, J.; Maurin, G.; Chang, J.-S.; Serre, C. Design of Hydrophilic Metal Organic Framework Water Adsorbents for Heat Reallocation. *Adv. Mater.* **2015**, *27*, 4775−4780.
(45) Permyakova, A.; Skrylnyk, O.; Courbon, E.; Affram, M.; Wang, S.; Lee, U.-H.; Valekar, A. H.; Nouar, F.; Mouchaham, G.; Devic, T.; De Weireld, G.; Chang, J.-S.; Steunou, N.; Frère, M.; Serre, C. "Synthesis Optimization, Shaping, and Heat Reallocation Evaluation of the Hydrophilic Metal−Organic Framework MIL-160(Al). *ChemSusChem* **2017**, *10*, 1419−1426.
(46) Leenders, M. Investigation of Metal Organic Frameworks for Seasonal Thermal Energy Storage Investigation of Metal Organic Frameworks for Seasonal Thermal Energy Storage, Master Thesis, University of Technology, 2017.
(47) Borges, D. D.; Normand, P.; Permiakova, A.; Babarao, R.; Heymans, N.; Galvao, D. S.; Serre, C.; De, W. G.; Maurin, G. Gas Adsorption and Separation by the Al-Based Metal-Organic Framework MIL-160. *J. Phys. Chem. C* **2017**, *121*, 26822−26832.
(48) Permyakova, A.; Wang, S.; Courbon, E.; Nouar, F.; Heymans, N.; D'Ans, P.; Barrier, N.; Billemont, P.; De Weireld, G.; Steunou, N.; Frère, M.; Serre, C. Design of salt-metal organic framework composites for seasonal heat storage applications. *J. Mater. Chem. A* **2017**, *5*, 12889−12898.
(49) Borges, D. D.; Maurin, G.; Galvaõ, D. S. Design of Porous Metal-Organic Frameworks for Adsorption Driven Thermal Batteries. *MRS Adv.* **2017**, *2*, 519−524.
(50) Choi, S.-J.; Kwon, T.-H.; Im, H.; Moon, D.-I.; Baek, D. J.; Seol, M.-L.; Duarte, J. P.; Choi, Y.-K. A polydimethylsiloxane (PDMS) sponge for the selective absorption of oil from water. *ACS Appl. Mater. Interfaces* **2011**, *3*, 4552−4556.
(51) Zhao, X.; Li, L.; Li, B.; Zhang, J.; Wang, A. Durable superhydrophobic/superoleophilic PDMS sponges and their applications in selective oil absorption and in plugging oil leakages. *J. Mater. Chem. A* **2014**, *2*, 18281−18287.
(52) Zhou, T.; Yang, J.; Zhu, D.; Zheng, J.; Handschuh-Wang, S.; Zhou, X.; Zhang, J.; Liu, Y.; Liu, Z.; He, C.; Zhou, X. Hydrophilic Sponges for Leaf-Inspired Continuous Pumping of Liquids. *Adv. Sci.* **2017**, *4*, 1700028.
(53) Kwon, D.; Lee, T.-I.; Shim, J.; Ryu, S.; Kim, M. S.; Kim, S.; Kim, T.-S.; Park, I. Highly Sensitive, Flexible, and Wearable Pressure Sensor Based on a Giant Piezocapacitive Effect of Three-Dimensional Microporous Elastomeric Dielectric Layer. *ACS Appl. Mater. Interfaces* **2016**, *8*, 16922−16931.
(54) Li, H.; Ding, Y.; Ha, H.; Shi, Y.; Peng, L.; Zhang, X.; Ellison, C. J.; Yu, G. An All-Stretchable-Component Sodium-Ion Full Battery. *Adv. Mater.* **2017**, *29*, 1700898.
(55) Kim, S.; Amjadi, M.; Lee, T.-I.; Jeong, Y.; Kwon, D.; Kim, M. S.; Kim, K.; Kim, T.-S.; Oh, Y. S.; Park, I. Wearable, Ultrawide-Range, and Bending-Insensitive Pressure Sensor Based on Carbon Nanotube Network-Coated Porous Elastomer Sponges for Human Interface and Healthcare Devices. *ACS Appl. Mater. Interfaces* **2019**, *11*, 23639−23648.
(56) Wang, T.; Li, X.; Dai, W.; Fang, Y.; Huang, H. Enhanced adsorption of dibenzothiophene with zinc/copper-based metal-organic frameworks. *J. Mater. Chem. A* **2015**, *3*, 21044−21050.
(57) Li, H.; Li, M.; Li, W.; Yang, Q.; Li, Y.; Gu, Z.; Song, Y. Three dimensional MOF-sponge for fast dynamic adsorption. *Phys. Chem. Chem. Phys.* **2017**, *19*, 5746−5752.
(58) Karra, J. R.; Walton, K. S. Molecular simulations and experimental studies of CO2, CO, and N2 adsorption in metal-organic frameworks. *J. Phys. Chem. C* **2010**, *114*, 15735−15740.
(59) Schlichte, K.; Kratzke, T.; Kaskel, S. Improved synthesis, thermal stability and catalytic properties of the metal-organic framework compound Cu3(BTC)2. *Microporous Mesoporous Mater.* **2004**, *73*, 81−88.
(60) Ahn, J.; Gu, J.; Hwang, B.; Kang, H.; Hwang, S.; Jeon, S.; Jeong, J.; Park, I. Printed fabric heater based on Ag nanowire/carbon nanotube composites. *Nanotechnology* **2019**, *30*, 455707.
(61) Ahn, J.; Jeong, Y.; Zhao, Z.; Hwang, S.; Kim, K.; Ko, J.; Jeon, S.; Park, J.; Kang, H.; Jeong, J. H.; Park, I. "Heterogeneous Conductance-Based Locally Shape-Morphable Soft Electrothermal Actuator. *Adv. Mater. Technol.* **2020**, *5*, 1900997.

https://dx.doi.org/10.1021/acsami.0c00143
ACS Appl. Mater. Interfaces 2020, 12, 13338−13347